PCCP

PAPER

View Article Online
View Journal | View Issue

Cite this: *Phys. Chem. Chem. Phys.*, 2014, **16**, 13932

Structure–properties relationship of carbazole and fluorene hybrid trimers: experimental and theoretical approaches†

Ausra Tomkeviciene,[a] Juozas V. Grazulevicius,*[a] Dmytro Volyniuk,[a] Vygintas Jankauskas[b] and Gjergji Sini[c]

Received 20th January 2014,
Accepted 28th April 2014

DOI: 10.1039/c4cp00302k

www.rsc.org/pccp

Synthesis and properties of fluorene and carbazole derivatives having three electrophores per molecule with different architectures are reported. The synthesized compounds possess high thermal stabilities with 5% weight loss temperatures exceeding 350 °C. They form glasses with glass transition temperatures ranging from 60 to 68 °C. Cyclovoltammetric experiments revealed the high electrochemical stability of the fluorene trimer. In contrast, 2- and 2,7-fluorenyl substituted carbazole derivatives show irreversible oxidation in the CV experiments. The electron photoemission spectra of the films of the synthesized compounds revealed ionization potentials of 5.65–5.89 eV. Hole drift mobilities in the amorphous layers of the synthesized compounds reach 10^{-2} cm^2 V^{-1} s^{-1} at high electric fields, as established by a xerographic time-of-flight technique. DFT calculations show that HOMO and LUMO orbitals of the compounds are very similar in energy and shape. The similar hole mobilities observed for the three compounds are discussed in the frame of the Marcus theory. An important influence of the alkyl groups on the ionization potentials and on the hole mobilities was also observed and its origin is discussed.

Introduction

Search for new materials with advanced properties is one of the major tasks of the rapidly developing field of organic optoelectronics. Much attention is being focused on conjugated compounds. Such conjugated systems are featured with interesting optical and photophysical properties and have a high potential for utilizing as materials in organic light-emitting diodes (OLEDs)[1] field effect transistors,[2] and solar cells.[3]

Due to the efficient hole transport and excellent thermal stability of carbazole derivatives, the electron-rich carbazole moiety is widely used in the design of charge-transporting and light-emitting materials.[4,5] Fluorene derivatives are also known to possess high emission quantum yields and exhibit ambipolar charge carrier transport properties.[6–8] The molecular design of new derivatives of carbazole and fluorene has mostly been focused on networking through 3,6-positions of carbazole and 2,7-positions of fluorene.[9,10] Most of these compounds are polymeric materials, and incomparably less research has been carried out on low-molar-mass 2,7-substituted carbazole or fluorene derivatives.[4,11–13] Making 2,7-substituted carbazole compounds is much more difficult, as compared to 3,6-substituted derivatives, since C3 and C6 positions of the carbazole moiety are activated by the nitrogen atom. All kinds of electrophilic substitution reactions can take place in these positions. Leclerc *et al.*[14,15] and Müllen *et al.*[16] reported convenient synthetic pathways towards 2,7-dihalocarbazoles, which are useful precursors for carbazole-based electroactive materials. As noted in the review,[9] while the class of 3,6-substituted carbazole derivatives was found to be very interesting for electrochemical and phosphorescence applications, the class of 2,7-substituted carbazoles showed promising optical properties in the visible range. It was also recognized that a major intrinsic difference between these two families of carbazole derivatives is the effective conjugation length, being larger for 2,7-carbazole compounds.[9] These findings stimulated the design of new 2,7-substituted carbazole derivatives with improved properties.

In this paper we report the results from joint experimental and theoretical approaches on the conjugated carbazole–fluorene

---

[a] *Department of Polymer Chemistry and Technology, Kaunas University of Technology, Radvilenu pl. 19, LT-50254, Kaunas, Lithuania. E-mail: juozas.grazulevicius@ktu.lt; Fax: +370 37 300152; Tel: +370 37 300193*

[b] *Department of Solid State Electronics, Vilnius University, Sauletekio al. 9, LT-10222 Vilnius, Lithuania*

[c] *Laboratoire de Physicochimie des Polymères et des Interfaces, EA 2528 Université de Cergy-Pontoise, 5 mail Gay-Lussac, 95031 Cergy-Pontoise Cedex, France*

† Electronic supplementary information (ESI) available: Frontier orbital pictograms and theoretical absorption spectra of **CFC1**, **CFC2**, and **R-CFC**, **R-FCF**, and **R-FFF** (R = H, CH_3) model compounds; optical and electronic parameters for **R-CFC**, **R-FCF**, and **R-FFF** (R = H, CH_3) model compounds. Normalized fluorescence spectra of the dilute (10^{-5} M) THF solutions of **CFC1**, **CFC2**, **FCF**, **FFF**. Fluorescence transients of dilute (10^{-5} M) THF solutions of **FCF**, **FFF**, and **CFC2**. DSC curves of **FFF** and **CFC2**. See DOI: 10.1039/c4cp00302k

hybrid trimers. The thermal, optical, electrochemical and photoelectrical properties of the trimers were investigated and are discussed in detail. A comparative analysis of some molecular parameters involved in the calculation of charge-transfer rate constants (k_{CT})[17–20] is applied. Aiming to distinguish between the intrinsic properties of these materials and the influence of the real alkyl groups, different model compounds replacing real alkyl groups with R = H, CH_3 are considered, along with real alkyl groups in the case of fluorene-containing trimers. Due to the negligible role of alkyl groups on the intrinsic properties of these molecules, the results corresponding to R = CH_3 or real groups are given in the ESI,† and only the results for R = H are presented in the main paper (except otherwise indicated). While the designing of new materials generally focuses on the electronic properties of the building blocks, we show that the nature of the alkyl chains may exhibit important influences other than morphology-related ones.

Experimental

Instrumentation

^1H and ^{13}C NMR spectra were recorded using Varrian Unity Inova [300 MHz (^1H), 75.4 MHz (^{13}C)] spectrometer at room temperature. All the data are given as chemical shifts in δ (ppm), $(CH_3)_4Si$ (TMS, 0 ppm) was used as an internal standard. The courses of the reactions were monitored by TLC Silicagel 60 F254 plates and developed with I_2 or UV radiation. Silica gel (grade 60, 63–200 mesh, 60 Å, Fluka) was used for column chromatography. The melting points were estimated using Electrothermal Mel-Temp melting point apparatus. The mass (MS) spectra were recorded on a Waters ZQ (Waters, Milford, MA). Elemental analysis was performed with Exeter Analytical CE-440 Elemental. Infrared (IR) spectra were recorded using Perkin Elmer Spectrum GX spectrometer. The spectra of the solid compounds were performed in KBr pellets.

Different scanning calorimetry (DSC) measurements were carried out using Perkin-Elmer DSC apparatus. Thermogravimetric analysis (TGA) was performed on a Mettler Toledo TGA/SDTA 851^e and Netzsch STA 409 with a data acquisition system 414/1. The DSC and TGA experiments were performed in a nitrogen atmosphere at a heating rate of 10 °C min^{-1}.

Ultraviolet absorption spectra of dilute solutions (10^{-5} M) of the synthesized compounds in tetrahydrofuran (THF) were recorded on Perkin Elmer Lambda 35 spectrophotometer. A microcell with an internal width of 1 mm. Fluorescence spectra were recorded with a Hitachi MPF-4 spectrometer (resolution 2 nm). A cell with an internal width of 10 mm and 10^{-5} M solutions of investigated compounds in THF was used for the measurements. The absorption spectra of the solid thin films were recorded with Aventes AvaSpec-2048XL spectrometer, while the fluorescence spectra of the solid samples and fluorescence decay curves of the solutions were recorded with an Edinburgh Instruments FLS980 spectrometer.

The cyclic voltammetry (CV) measurements were carried out by a three-electrode assembly cell from Bio-Logic SAS and a micro-AUTOLAB Type III potentiostat-galvanostat. The working electrode was a glassy carbon with 0.12 cm^2 surface although the reference electrode and the counter electrode were Ag/Ag^+ 0.01 M and Pt wire, respectively. Solutions with concentration 10^{-3} M of the compounds in argon-purged dichloromethane (Fluka) with tetrabutylammonium perchlorate (TBAP; 0.1 M) as electrolyte were used for the CV measurements.

The ionization potentials ($I_{p(EP)}$) of films of the synthesized compounds were measured by an electron photoemission in air method, as described before.[21] The measurement error is evaluated as 0.03 eV. The samples for the measurements were prepared by dissolving the compounds in THF and by casting on aluminum (Al) plates pre-coated with *ca.* 0.5 μm thick adhesive layer of the copolymer of methylmethacrylate and methacrylic acid. The measurement method is, in principle, similar to that described in the literature.[22] Hole drift mobilities were measured by xerographic time of flight technique (XTOF).[23,24] The samples for the measurements were prepared by drop casting of solutions of the compounds in THF onto a polyester film with Al layer.[25]

Materials

4-Bromo-2′-nitrobiphenyl,[26] 2-bromocarbazole,[26] 2-bromo-9-ethylcarbazole,[27] 2-(4,4,5,5-tetramethyl-1,3,2-dioxaborolan-2-yl)-9-ethylcarbazole, 4,4′-dibromo-2-nitrobiphenyl,[16] 2,7-dibromocarbazole,[16] 2,7-dibromo-9-(2-ethylhexyl)carbazole,[16] 2-bromo-9,9-diethylfluorene,[28] 2-(4,4,5,5-tetramethyl-1,3,2-dioxaborolan-2-yl)-9,9-diethylfluorene,[28] 2,7-dibromo-9,9-di(2-ethylhexyl)fluorene,[29] 2,7-dibromo-9,9-dihexylfluorene[30] were prepared according to published procedures.

General procedure for the synthesis of the derivatives of fluorene and carbazole by Suzuki coupling

Dibromoaryl derivative (1.8 mmol) and arylboronate (5.4 mmol) were dissolved in 40 ml of toluene. 10 ml of 2 M K_2CO_3 aqueous solution and tetra-*n*-butylammonium chloride (0.036 mmol) were added to the reaction mixture degassed by three subsequent freeze–thaw cycles. Thereafter, tri-*tert*-butylphosphine (0.036 mmol) and tetrakis(triphenylphosphine)palladium(0) (0.18 mmol) were added under argon. The mixture was stirred for 24 h at 110 °C. After cooling, the reaction mixture was diluted with ethyl acetate and the organic phase was washed with water and brine. After being dried over Na_2SO_4 and filtered, the solvent was removed and the crude product was purified by column chromatography.

2,7-Bis(9-ethylcarbazol-2-yl)-9,9-di(2-ethylhexyl)fluorene (CFC1). **CFC1** was prepared according to the general procedure using 2,7-dibromo-9,9-di(2-ethylhexyl)fluorene, and 2-(4,4,5,5-tetramethyl-1,3,2-dioxaborolan-2-yl)-9-ethylcarbazole. The crude product was purified by column chromatography on silica gel using hexane/dichloromethane (20/1) as an eluent. The target compound was obtained as white powder (fw = 776 g mol^{-1}) in 65% yield. ^1H NMR (300 MHz, $CDCl_3$), δ (ppm): 0.62–0.74 (m, 12H, CH_3), 0.80–1.11 (m, 18H, CH_2, CH), 1.54 (t, J = 7.0 Hz, 6H, CH_3), 2.19 (m, 4H, C–CH_2), 4.49 (q, J = 7.3 Hz, 4H, N–CH_2), 7.30 (d, J = 7.3 Hz, 2H, Ar), 7.46–7.62 (m, 6H, Ar), 7.67 (t, J = 5.0 Hz, 2H, Ar), 7.74–7.80 (m, 4H, Ar), 7.86 (d, J = 7.7 Hz, 2H, Ar), 8.20 (d, J = 4.0 Hz, 2H, Ar), 8.23 (s, 2H, Ar). ^{13}C NMR (75.4 MHz, $CDCl_3$), δ (ppm): 10.7 (CH_3), 14.1 (CH_3), 14.3 (CH_3), 23.0 (CH_2), 27.4 (CH_2), 28.5 (CH_2), 34.3 (CH_2), 35.0 (CH_2), 37.8 (CH), 44.8 (N–CH_2), 55.4 (C–CH_2), 107.2, 108.7, 118.9, 119.2, 120.1, 120.7, 120.8, 122.3, 123.1, 123.5, 123.6, 123.7, 125.8, 126.9, 140.3, 140.5, 140.7, 151.5. IR ν_{max} in cm^{-1} (KBr): (C–H Ar) 3054; (C–H) 2951, 2921, 2854; (C=C Ar) 1472, 1454; (C–H Ar) 807, 744, 724. MS (APCl$^+$, 20 V), *m*/*z* (%) = 777 ([M + H]$^+$, 100). Elemental analysis calcd for $C_{57}H_{64}N_2$ (%): C 88.09, H 8.30, N 3.60. Found (%): C 88.99, H 8.90, N 3.95.

2,7-Bis(9-ethylcarbazol-2-yl)-9,9-dihexylfluorene (CFC2). CFC2 was prepared according to the general procedure using 2,7-(dibromo-9,9-dihexyl)fluorene, and 2-(4,4,5,5-tetramethyl-1,3,2-dioxaborolan-2-yl)-9-ethylcarbazole. The crude product was purified by column chromatography on silica gel using hexane/ethyl acetate (20/1) as an eluent. The target compound was obtained as white powder (fw = 720 g mol^{-1}) in 72% yield. ^1H NMR (300 MHz, $CDCl_3$), δ (ppm): 0.84 (t, *J* = 7.1 Hz, 6H, CH_3), 0.88–0.95 (m, 4H, CH_2), 1.13–1.24 (m, 12H, CH_2), 1.58 (t, *J* = 7.2 Hz, 6H, CH_3), 2.19 (m, 4H, C–CH_2), 4.52 (q, *J* = 7.1 Hz, 4H, N–CH_2), 7.32 (t, *J* = 6.8 Hz, 2H, Ar), 7.49–7.57 (m, 4H, Ar), 7.64 (dd, J_1 = 8.0 Hz, J_2 = 1.4 Hz, 2H, Ar), 7.74 (s, 2H, Ar), 7.80 (d, *J* = 9.2 Hz, 4H, Ar), 7.91 (d, *J* = 7.8 Hz, 2H, Ar), 8.21 (d, *J* = 7.6 Hz, 2H, Ar), 8.26 (d, *J* = 8.0 Hz, 2H, Ar). ^{13}C NMR (75.4 MHz, $CDCl_3$), δ (ppm): 14.0 (CH_3), 14.1 (CH_3), 22.7 (CH_2), 24.0 (CH_2), 29.8 (CH_2), 31.6 (CH_2), 37.6 (C–CH_2), 40.5 (N–CH_2), 55.4 (C–CH_2), 106.9, 108.6, 118.8, 119.0, 120.0, 120.5, 120.7, 122.0, 122.2, 122.9, 125.7, 126.6, 139.7, 140.0, 140.5, 140.6, 141.2, 151.8. IR ν_{max} in cm^{-1} (KBr): (C–H Ar) 3059; (C–H) 2953, 2925, 2853; (C=C Ar) 1468, 1450; (C–H Ar) 810, 761, 731. MS (APCl$^+$, 20 V), *m*/*z* (%) = 721 ([M + H]$^+$, 100). Elemental analysis calcd for $C_{53}H_{56}N_2$ (%): C 88.29, H 7.83, N 3.89. Found (%): C 88.87, H 8.32, N 4.01.

2,7-Bis(9,9-diethylfluoren-2-yl)-9-(2-ethylhexyl)carbazole (FCF). FCF was prepared according to the general procedure using 2,7-dibromo-9-(2-ethylhexyl)carbazole and 2-(4,4,5,5-tetramethyl-1,3,2-dioxaborolan-2-yl)-9,9-diethylfluorene. The crude product was purified by column chromatography on silica gel using hexane/dichloromethane (10/1) as an eluent. The product was crystallized from the eluent mixture of solvents and was obtained as white crystals (fw = 719 g mol^{-1}, mp = 174–175 °C) in 75% yield. ^1H NMR (300 MHz, $CDCl_3$), δ (ppm): 0.47 (t, *J* = 7.3 Hz, 12H, CH_3), 0.95 (t, *J* = 7.3 Hz, 3H, CH_3), 1.05 (t, *J* = 7.3 Hz, 3H, CH_3), 1.37–1.44 (m, 2H, CH_2), 1.47–1.54 (m, 6H, CH_2), 2.12–2.20 (m, 9H, C–CH_2, CH), 4.37 (d, *J* = 7.3 Hz, 2H, N–CH_2), 7.37–7.44 (m, 6H, Ar), 7.61 (dd, *J* = 1.5 Hz, *J* = 8.0 Hz, 2H, Ar), 7.71–7.88 (m, 10H, Ar), 8.21 (d, *J* = 8.0 Hz, 2H, Ar). ^{13}C NMR (75.4 MHz, $CDCl_3$), δ (ppm): 8.9 (CH_3), 11.3 (CH_3), 14.4 (CH_3), 23.4 (CH_2), 24.8 (CH_2), 29.2 (CH_2), 31.4 (CH_2), 33.1 (CH_2), 39.9 (CH), 47.5 (N–CH_2), 56.5 (C–CH_2), 107.8, 119.0, 120.0, 120.2, 120.8, 122.2, 123.2, 126.6, 127.1, 127.3, 139.8, 140.9, 141.4, 142.4, 150.5, 150.9. IR ν_{max} in cm^{-1} (KBr): (C–H Ar) 3098, 3008; (C–H) 2962, 2920, 2875, 2850;(C=C Ar) 1464, 1446; (C–H Ar) 820, 770, 737. MS (APCl$^+$, 20 V), *m*/*z* (%) = 720 ([M + H]$^+$, 100). Elemental analysis calcd for $C_{54}H_{57}N$ (%): C 90.08, H 7.98, N 1.95. Found (%): C 89.11, H 8.00, N 2.11.

2,7-Bis(9,9-diethylfluoren-2-yl)-9,9-di(2-ethylhexyl)fluorene (FFF). FFF was prepared according to the general procedure using 2,7-dibromo-9,9-dihexylfluorene and 2-(4,4,5,5-tetramethyl-1,3,2-dioxaborolan-2-yl)-9,9-diethylfluorene. The crude product was purified by column chromatography on silica gel using hexane/acetone (20/1) as an eluent. The product was crystallized from the eluent mixture of solvents and was obtained as white crystals (fw = 774 g mol^{-1}, mp = 101–102 °C) in 72% yield. ^1H NMR (300 MHz, $CDCl_3$), δ (ppm): 0.45 (t, *J* = 7.3 Hz, 12H, CH_3), 0.79–0.83 (m, 10H, CH_3, CH_2), 1.10–1.21 (m, 12H, CH_2), 2.15 (q, *J* = 7.0 Hz, 12H, C–CH_2), 7.36–7.44 (m, 6H, Ar), 7.67–7.72 (m, 8H, Ar), 7.78–7.86 (m, 6H, Ar). ^{13}C NMR (75.4 MHz, $CDCl_3$), δ (ppm): 8.9 (CH_3), 14.3 (CH_3), 22.8 (CH_2), 24.1 (CH_2), 29.9 (CH_2), 31.7 (CH_2), 33.1 (CH_2), 40.6 (CH_2), 55.6 (C–CH_2), 119.9, 120.1, 121.7, 123.2, 126.4, 127.3, 140.3, 140.7, 140.8, 141.0, 141.5, 150.4, 150.9. IR ν_{max} in cm^{-1} (KBr): (C–H Ar) 3061, 3036; (C–H) 2958, 2928, 2850; (C=C Ar) 1466, 1449; (C–H Ar) 814, 770, 738. MS (APCl$^+$, 20 V), *m*/*z* (%) = 775 ([M + H]$^+$, 100). Elemental analysis calcd for $C_{59}H_{66}$ (%): C 91.42, H 8.58. Found (%): C 91.95, H 9.40.

Computational details

All computations were performed at the density functional theory (DFT) level[31] by employing the B3LYP[32,33] functional, in conjunction with the 6-31G(d,p) basis set. The geometry optimizations (followed by frequency calculations) of the model compounds **R-FFF**, **R-FCF**, and **R-CFC** (R = H, CH_3) were performed in absence of medium effects. While test calculations on **CFC1**, **CFC2** (containing real alkyl groups) and **R-CFC**, **R-FCF**, **R-FFF** (R = H, CH_3) result in insignificant changes in the electronic structure and optical spectra (Fig. S1 and Table S1, ESI†), the numerical results presented in the manuscript correspond to model compounds **H-CFC**, **H-FCF**, and **H-FFF**. The aim of this choice is to better distinguish between the intrinsic properties of these compounds (bare molecular cores) on the one hand, and the influence of the real alkyl chains on the other. The results showing the (lack of significant) influence of the alkyl groups in the intrinsic optical and electronic properties of these compounds are collected in Fig. S1 and Tables S1 and S2 (ESI†).

The spectroscopic properties of the molecules were calculated by using a time dependent density functional theory method (TDDFT)[34–37] in absence of medium effects. Up to 20 excited states were calculated and the theoretical absorption bands were obtained by considering a band half-width of 0.2 eV at half-height.[38]

The vertical and adiabatic ionization potentials (I_p) were calculated "in the gas phase" at the B3LYP/6-31G(d,p) level as differences of the total energies between the neutral species and the cationic species.

The internal reorganization energy (λ_i) values were calculated at the B3LYP/6-31G(d,p) level according to the following equation:[39]

$$\begin{aligned}\lambda_i &= \lambda_i^1 + \lambda_i^2 \\ &= \left(E_M^{\mathrm{Geom(M^+)}} - E_M^{\mathrm{Geom(M)}}\right) + \left(E_{M^+}^{\mathrm{Geom(M)}} - E_{M^+}^{\mathrm{Geom(M^+)}}\right)\end{aligned}$$

in which the quantity $E_{M^+}^{\mathrm{Geom(M)}}$ for instance corresponds to the energy of the cationic species (M^+) in the geometry of the neutral molecule (M).

Test calculations considering the solvent effect (THF, ε = 7.43) were carried out by using the conductor-like polarizable continuum model (CPCM).[40,41] Our results indicate qualitatively insignificant influence of the solvent effect on the geometries of the neutral compounds and on their relative optical absorption spectra and dipole moments (Fig. S1d and e and Table S2, ESI†). In the following, if not otherwise indicated, only the ''gas phase'' results are presented.

Finally, we note that restricted open shell Hartree–Fock (roHF) calculations were performed in order to check if charge-localization could occur in these compounds. While ''gas phase'' calculations resulted in preferential symmetrical structures, the consideration of the solvent effect, as expected, allows to obtain stable asymmetric structures. Similar calculations at the unrestricted open shell Hartree–Fock (UHF) level result in heavily spin-contaminated states.

All computations were performed with the Gaussian 09 program.[42]

Results and discussion

Synthesis

The starting compounds 2,7-dibromo-9,9-di(2-ethylhexyl)fluorene (**1**), 2,7-dibromo-9-(2-ethylhexyl)carbazole (**2**), 2,7-dibromo-9,9-dihexylfluorene (**3**), 2-(4,4,5,5-tetramethyl-1,3,2-dioxaborolan-2-yl)-9-ethylcarbazole (**4**) and 2-(4,4,5,5-tetramethyl-1,3,2-dioxaborolan-2-yl)-9,9-diethylfluorene (**5**) were synthesized according to the published procedures.[26–30] Pd-catalyzed Suzuki coupling reactions of dibromo compounds and arylboronates were accomplished by adding a catalytic amount of bulky tri-*tert*-butylphosphine as a promoter to afford the target compound with a carbazole core (**FCF**) as well as the compounds with a fluorene core (**CFC**, **FFF**) in good yields (Scheme 1). ^{1}H and ^{13}C NMR, mass spectrometries and elemental analysis confirmed the chemical structures of the compounds.

Geometries and frontier orbitals

The geometries of the model compounds **H-FFF**, **H-FCF**, and **H-CFC** (containing methyl groups instead of the experimental alkyl groups), along with the geometries of **CFC1** and **CFC2** containing real alkyl groups, are presented in Fig. 1.

The three model compounds exhibit similar structures, with inter-ring dihedral angles of 37.8° in the case of **H-CFC** and **H-FCF**, and 37.4° in the case of **H-FFF** (37.9° and 37.8° for **CFC1** and **CFC2** respectively). These dihedral angles decrease to 27.8, 27.8, and 27.4°, respectively, upon oxidation. In the three cases only the isomers corresponding to *trans*-orientation between adjacent unities are presented. The corresponding *cis*-isomers are expected to present a steric hindrance between the alkyl chains of the adjacent unities, thus being less probable.

The frontier orbitals for the three molecules (Fig. 2) are very similar for all compounds, being principally localized on the central core, but containing important contributions from the lateral ones. The electronic properties related to these orbitals are consequently expected to exhibit similarities.

It is worth noting that the geometrical parameters and frontier orbital distributions are found to be insignificantly dependent on the nature of the real alkyl chains (Fig. S1a, ESI†).

Thermal properties

The thermal stability and morphological changes of the synthesized compounds were studied by TGA and DSC, respectively. The melting points and glass transition temperatures of the derivatives are summarized in Table 1. **FFF**, **CFC** and **FCF** exhibited a relatively high thermal stability with 5% weight loss temperature (T_{ID}) of over 350 °C. The DSC measurements showed that the synthesized compounds are able to form molecular glasses. The fluorene trimer (**FFF**) and the compound end-capped with fluorene moieties (**FCF**) were isolated after the synthesis as crystalline materials and their first DSC heating scans revealed endothermal melting signals. However no crystallization was observed during the cooling scans, which indicated a transition from the melt to the glassy state. In the second and the following DSC heating scans, **FFF** and **FCF** exhibited glass transitions at 60 and 68 °C, respectively. The compounds end-capped with carbazole moieties (**CFC**) showed

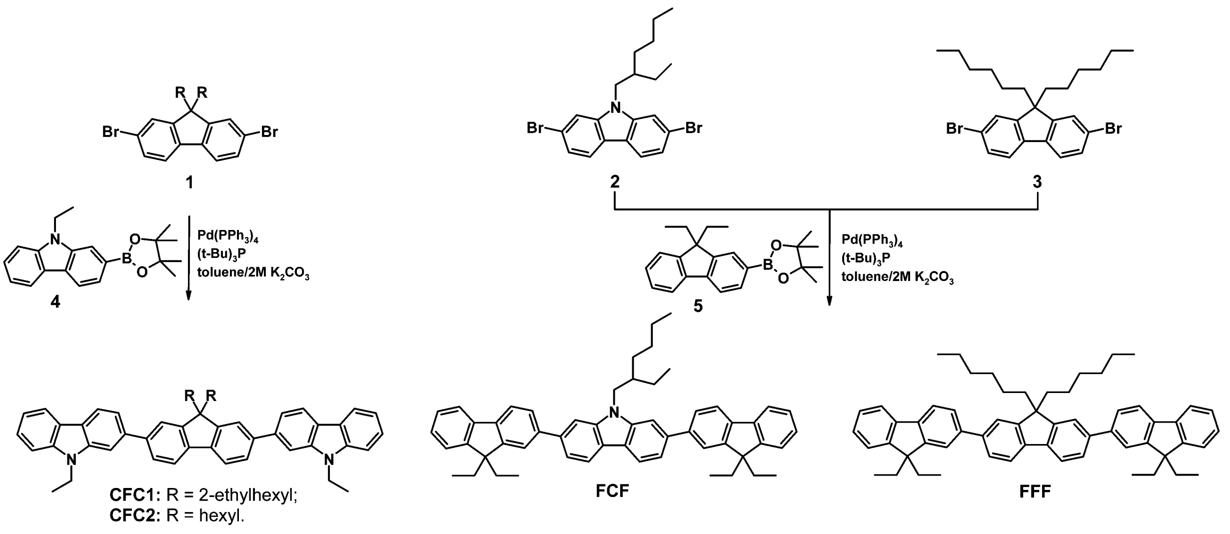

Scheme 1 Synthesis of **CFC1**, **CFC2**, **FCF** and **FFF**.

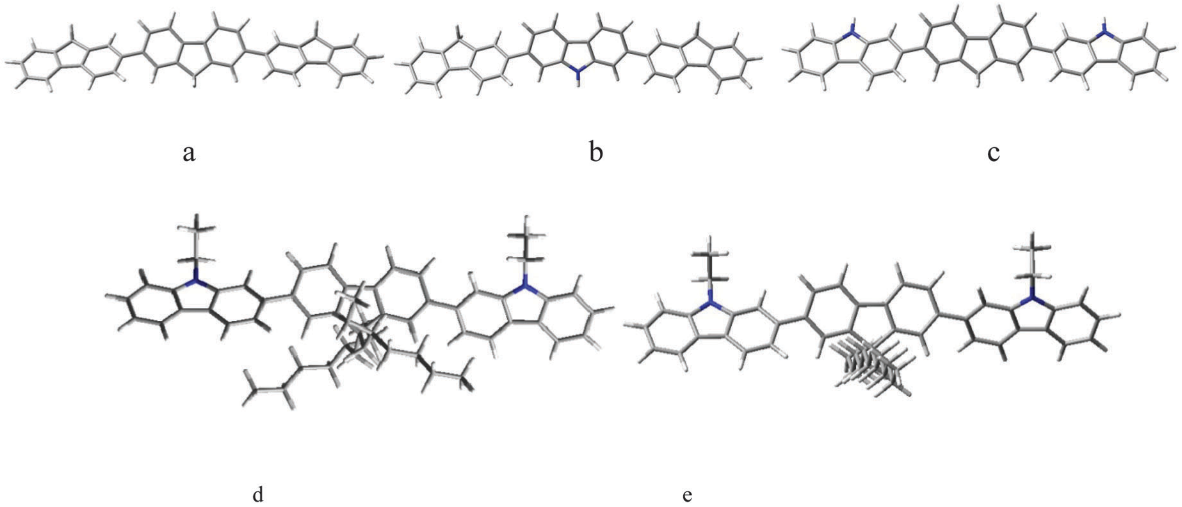

Fig. 1 Optimized geometries of (a) **H-FFF**, (b) **H-FCF**, and (c) **H-CFC** model compounds, and (d and e) optimized geometries of **CFC1** and **CFC2** compounds containing real alkyl chains, obtained at the B3LYP/6-31G(d,p) level (in the absence of medium effect).

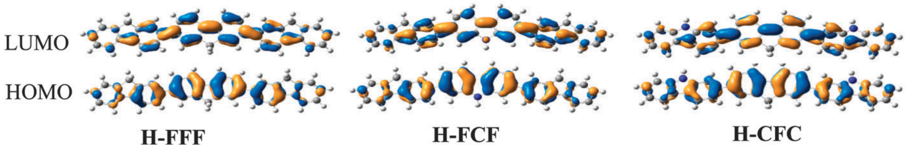

Fig. 2 Pictograms of HOMO and LUMO orbitals corresponding to **H-FFF**, **H-FCF**, and **H-CFC** model compounds.

Table 1 Thermal characteristics of **CFC1**, **CFC2**, **FCF**, **FFF**[a]

Compound	T_m [°C]	T_g [°C]	T_{ID} [°C]
CFC1	—[b]	68	415
CFC2	—[b]	61	371
FCF	173[c]	68	432
FFF	106[c]	60	388

[a] T_g: glass-transition temperatures, T_m: melting temperatures, T_{ID}: 5% weight loss temperatures. [b] Obtained as an amorphous material. [c] The melting point was only detected during the first heating.

different behaviour in the DSC measurements. Only the glass transition was observed in repeated DSC scans, and no peaks appeared due to crystallization and melting (Fig. 3). The amorphous nature of **CFC1** and **CFC2** can be explained by the relatively loose packing of the molecules.

The change of the alkyl fragment from hexyl (**CFC2**) to 2-ethylhexyl (**CFC1**), leads to an increase of the glass-transition temperature (T_g) by 7 °C. This observation can apparently be explained by the slightly higher molecular weight of **CFC1** and the stronger intermolecular interaction in its glassy samples.

Optical and photophysical properties

UV absorption and fluorescence spectra of the dilute solutions of **CFC1**, **CFC2**, **FCF**, and **FFF** in THF are shown in Fig. 4 and Fig. S4 (ESI†) respectively. The wavelengths of the absorption

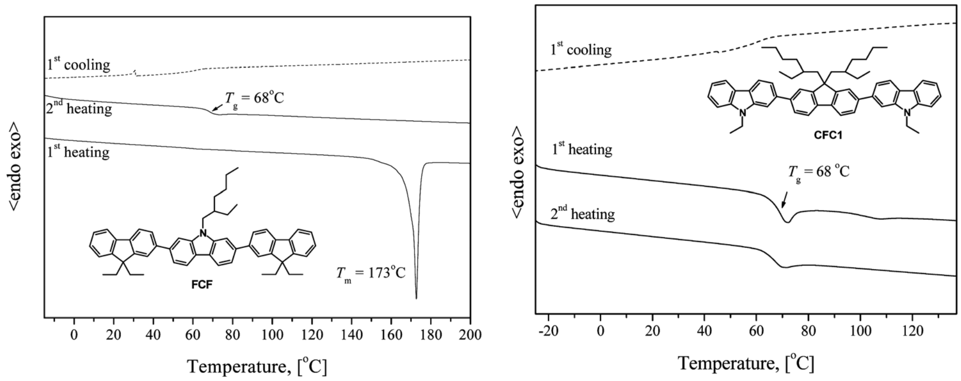

Fig. 3 DSC curves of **FCF** and **CFC1** (heating rate 10 °C min^{-1}, N_2 atmosphere).

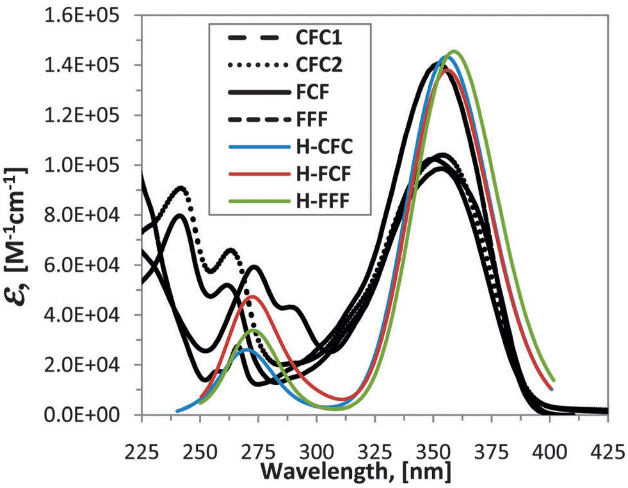

Fig. 4 Experimental absorption spectra of 10^{-5} M THF solutions of **CFC1**, **CFC2**, **FCF**, **FFF** (black curves) and theoretical ones (colored curves, corresponding to **H-CFC**, **H-FCF**, **H-FFF**) obtained by mean of TD-B3LYP/6-31G(d,p) calculations "in gas phase".

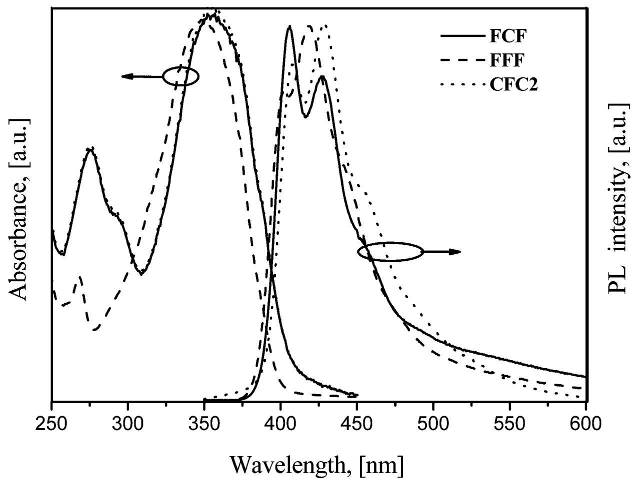

Fig. 5 Absorption and fluorescence spectra of the solid films of **FCF**, **FFF**, and **CFC2**.

and fluorescence maxima, the values of the extinction coefficient, the optical band gaps, and the fluorescence lifetimes of the compounds are summarized in Table 2.

The UV spectra of these compounds are similar. The molar extinction coefficients (ε) of compounds **CFC1, CFC2** and **FCF** containing carbazole moieties are similar. The fluorene trimer (**FFF**) exhibit higher values of the molar extinction coefficient and a slightly higher optical band gap.

The TD-B3LYP absorption spectra for model compounds **H-CFC**, **H-FCF**, and **H-FFF** are also shown in Fig. 4 (see Fig. S1c and d, ESI† for the theoretical absorption spectra of **M-CFC**, **M-FCF**, and **M-FFF**). The $S_0 \rightarrow S_1$ excitations are entirely due to HOMO → LUMO electronic transition for the three compounds (Fig. S2, ESI†). The almost identical low-energy band-maxima positions across the series (Fig. 4) are consistent with the similarities of the frontier orbitals (Fig. 2) and their energy gap for the three compounds (Table 2). However, differences in band intensities of **CFC**, **FCF**, and **FFF** are observed experimentally, the absorption being more intense in the case of **FFF**. This last experimental difference is not reproduced in the theoretical spectra regardless of the presence of real alkyl chains and the solvent influence in the calculations (Fig. S1e, ESI†), suggesting that differences in the solute–solute and/or solute–solvent interactions might be in play. The reason for these differences might be traced back to the stronger dipole moment of **H-CFC** (2.8 D) as compared to 0.7 D for **H-FFF** (3.7 D and 0.6 D for **CFC1** and **FFF** respectively, Table S2, ESI†), and to the smaller steric hindrance from the alkyl chains in the central unit of **FCF**. The same assumption may also explain the difference in the optical band-gap trends observed between the experimental (**FFF** > **FCF** = **CFC**) and theoretical (**H-FFF** < **H-FCF** = **H-CFC**) ones. However, both trends are quite negligible (roughly 0.03 eV, 3 nm, Table 2), which is out of reach of the theoretical level applied in this study.

The triplet energies of the three compounds were also calculated (Table S3, ESI†) indicating only a slight global increase (by 0.07 eV) in the order **H-FFF** < **H-CFC** < **H-FCF**. However, these values remain relatively low (2.55–2.62 eV and 2.20–2.29 eV for the vertical and relaxed T_1 energies, respectively) as compared to roughly 2.9–3.0 eV, which is a desired low-limit value for efficient blue phosphorescent OLEDs. It is worth noting that the intrinsic influence of the real alkyl chains on the triplet energies is found negligible (Table S3, ESI†).

The absorption and fluorescence measurements of the thin films of compounds **CFC2**, **FCF**, and **FFF** were also performed (Fig. 5). The wavelengths of the absorption and fluorescence

Table 2 Photophysical characteristics of 10^{-5} M THF solutions and thin films of **CFC1**, **CFC2**, **FCF**, and **FFF**

	Solution					Solid film	
Compound	$\lambda_{\text{abs.}}{}^{a}$ [nm]	ε^{b} [M^{-1} cm^{-1}]	$\lambda_{\text{f}}^{\max c}$ [nm]	τ^{d} [ns]	$E_{\text{g}}^{\text{opt}\, e}$ [V]	$\lambda_{\text{abs.}}$ [nm]	$\lambda_{\text{f}}^{\max c}$ [nm]
CFC1	353 (356)	98 346	357, 413	—	3.16	—	—
CFC2	354	104 010	395, 416	0.65	3.16	356	405, 429
FCF	349 (356)	102 340	397, 417	0.70	3.16	356	406, 427
FFF	352 (359)	140 564	394, 415	0.30	3.19	350	402, 419

[a] Wavelengths of the absorption maxima of the solutions in THF (10^{-5} M) (theoretical $S_0 \rightarrow S_1$ absorption wavelengths in parentheses corresponding to **H-CFC, H-FCF, H-FFF** obtained at TD-B3LYP/6-31G(d,p) level "in gas phase"). [b] Molar extinction coefficients. [c] Wavelengths of the fluorescence intensity maxima. [d] Fluorescence lifetime. [e] Optical band gaps $E_{\text{g}}^{\text{opt}}$ estimated from the edges of the electronic absorption spectra.

Table 3 Electrochemical and photoelectrical characteristics of **CFC1**, **CFC2**, **FCF**, and **FFF**

Compound	$E_{ox}^{onset\,a}$ [V]	$I_{p(CV)}{}^{b}$ [eV]	$E_{A(CV)}{}^{b}$ [eV]	$I_{p(EP)}{}^{c}$ [eV]	$\varepsilon^{HOMO\,d}$ [eV]	$\varepsilon^{LUMO\,d}$ [eV]
CFC1	0.86	5.66	−2.50	5.83 (6.09)	−5.17	−1.30
CFC2	0.91	5.71	−2.55	5.85		
FCF	0.88	5.68	−2.52	5.65 (6.11)	−5.19	−1.31
FFF	0.94	5.74	−2.55	5.89 (6.13)	−5.21	−1.36

[a] The onset oxidation potentials E_{ox}^{onset} are measured by cyclic voltamperometry from the first redox cycle. [b] Ionization potentials $I_{p(CV)}$ and electron affinities $E_{A(CV)}$ were estimated by cyclic voltamperometry data according to $I_{p(CV)} = 4.8 + E_{ox}^{onset}$ and $E_{A(CV)} = -(I_{p(CV)} - E_g^{opt})$. [c] The ionization potentials $I_{p(EP)}$ were measured by electron photoemission in air method from films (in parenthesis theoretical adiabatic I_p values corresponding to **H-CFC**, **H-FCF**, **H-FFF** obtained at B3LYP/6-31G(d,p) level "in gas phase"). [d] HOMO and LUMO energies of **H-CFC**, **H-FCF**, **H-FFF** as calculated at the B3LYP/6-31G(d,p) level "in gas phase".

maxima are listed in Table 2. Essentially, the shape of the absorption and fluorescence bands of the derivatives remained unchanged for the films, as compared to those observed for the solutions; however, red shifts (up to 7 nm for absorption and up to 13 nm for fluorescence) and negligible broadening of the bands were observed indicating enhanced intermolecular interactions in the solid state.

To get an insight into the excited state relaxation processes of the synthesized compounds, fluorescence decay curves of dilute solutions of **CFC2**, **FCF**, and **FCF** were recorded (Fig. S5, ESI†). The fluorescence transients of the dilute (10^{-5} M) THF solutions of **CFC2**, **FCF**, and **FCF** compounds express single exponential decays. Reduced χ^2 values, which were used together with weighted residuals as the goodness-of-fit criteria, did not exceed 1.3, ensuring a reliable description of the experimental data. The fluorescence lifetimes (τ) of the dilute THF solutions varied from ~0.3 ns for **FCF** to ~0.7 ns for **CFC2** and **FCF** (Table 2).

Electrochemical properties and ionization potentials

To elucidate the energetic conditions for energy and electron transfer in dilute solutions, the ionization potentials and electron affinities were established by cyclic voltamperometry. The measurements were carried out with a glassy carbon electrode in dichloromethane solutions containing 0.1 M tetrabutylammonium perchlorate (TBAP) as electrolyte, Ag/AgNO$_3$ as the reference electrode and a Pt wire counter electrode. The electrochemical characteristics are summarized in Table 3. The CV curves of **FFF**, **CFC1**, and **FCF** are shown in Fig. 6. The CV measurements of the fluorene trimer (**FFF**) revealed a fully reversible oxidation peak at 1.06 V. Repeated oxidation and reduction had no influence on the redox potentials. This observation confirms the electrochemical stability of the compound. The ionization potential ($I_{p(CV)}$) of **FFF** was found to be 5.74 eV (Table 2). With the band gap (E_g^{opt}) value obtained from the absorption spectrum, an electron affinity ($E_{A(CV)}$) value of −2.55 eV was estimated for **FFF**.

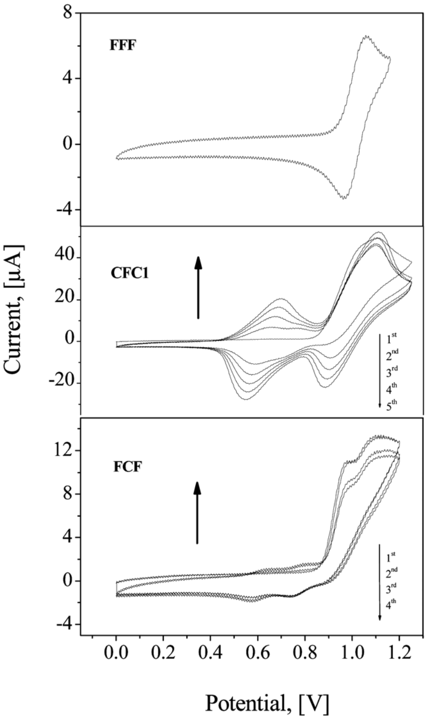

Fig. 6 Cyclic voltammograms of **FFF**, **CFC1** and **FCF** in argon-purged dichloromethane solution (scan rate of 50 mV s^{-1}).

CV measurements of the compound end-capped with carbazole moieties (**CFC1**) revealed completely different results. In the first redox cycle an oxidation of **CFC1** with the onset at 0.86 V was observed. E_{ox}^{onset} of **CFC1** was found to be somewhat lower than that of the fluorene trimer **FFF** (0.94 V). As the CV scans were continued, **CFC1** exhibited two oxidation peaks in the region of 0.69–1.11 V, instead of only one (0.86 V) in the first cycle. Presumably, the carbazole moieties were oxidized in the first scan, followed by an irreversible formation of a new carbazolyl compound.[43] The peaks shifted to a higher potential field as the CV scans were continued. The film of the compound was apparently formed on the working electrode surface, and the film thickness gradually increased upon CV scanning. The potential shift of this maximum provided information on the increase of electrical resistance of the film.[43] **CFC1** exhibited two reduction peaks in the region of 0.55–0.88 V. **FCF** exhibited a similar electrochemical behavior. Obviously the electrochemical oxidation of 2- or 2,7-substituted carbazole compounds is not reversible, which means that such compounds are not electrochemically stable. The electrochemical oxidation of 3,6-substituted carbazole derivatives is reversible[12,44] as that of fluorene trimer (**FFF**). The different electrochemical behaviour of the 2,7-substituted carbazole compounds can apparently be explained by the donor effect of the carbazole nitrogen, due to which the 3,6-positions of 2,7-substituted carbazole compounds are highly activated and can undergo dimerization reactions.[45] Possible charge localization upon oxidation on only one carbazole unit in **CFC1** cannot be excluded, as has been assumed in the case of poly(*N*-octyl-2,7-carbazolediyl), probably giving rise to subsequent coupling reactions.[45]

As a means of checking for this last assumption, the geometries of **H-CFC** and **CFC1** in their cationic state have been optimized at the restricted open shell Hartree–Fock (roHF) level by taking into account the effect of the solvent (THF). Asymmetric geometries were obtained in both cases with HOMO distribution localized on only one carbazole unit (Fig. S3, ESI†), thus supporting the charge-localization assumption. A similar theoretical approach in the case of **H-FCF** and **H-FFF** results in preferential asymmetric **H-FCF** and symmetric **H-FFF** geometries, again in line with the electrochemical instability of **FCF** and the electrochemical stability of **FFF** in their oxidized state (for additional information see the legend of Fig. S3, ESI†).[46]

The $I_{p(CV)}$ values of all synthesized compounds are comparable (5.66–5.74 eV). The electron affinity ($E_{A(CV)}$) values of the compounds are also close and range from −2.55 to −2.50 eV.

The ionization potentials ($I_{p(EP)}$) of the solid layers of the synthesized compounds were also estimated by electron photoemission using the air method. The results are presented in Table 3. Usually the photoemission experiments are carried out in vacuum, and high vacuum is one of the main requirements for these measurements. If the vacuum is not high enough, the sample surface oxidation and gas adsorption influence the measurement results. In our case, however, the organic materials investigated are stable enough with respect to oxygen and the measurements could be carried out in air. The values of $I_{p(EP)}$ of the compounds with a fluorene core (**CFC**, **FFF**) are comparable (5.83–5.89 eV). Meanwhile, the compound having a carbazole core (**FCF**) showed a lower ionization potential of 5.65 eV. While the $I_{p(EP)}$ values are slightly larger than the corresponding ones obtained by CV ($I_{p(CV)}$), both methods indicate small ranges between the I_p values of the three compounds (0.08 and 0.24 eV for the CV and electron photoemission results, respectively).

The small range of I_p values seems to be reproduced also by the theoretical results ($\Delta I_p \sim 0.04$ eV), which can be explained by the similar space-distribution of HOMO orbitals of **H-CFC**, **H-FCF**, and **H-FFF** (Fig. 2). The I_p values deduced from the Koopmans' theorem ($-\varepsilon^{\mathrm{HOMO}}$ values, Table 3) also range in a small window (~0.05 eV). However, the theoretical I_p values increase in the order **H-CFC** < **H-FCF** < **H-FFF**, which remains unchanged if methyl groups are considered instead of hydrogen atoms (Table S1, ESI†). Consequently, it can be concluded that the smaller $I_{p(EC)}$ and $I_{p(EP)}$ values corresponding to **FCF** as compared to **CFC2** should not stem from their intrinsic molecular properties. A possible explanation might again come from stronger intermolecular interactions in the case of **FCF**, probably due to a smaller steric hindrance from the alkyl chain in the central unit.

We conclude this point by underlying that the relevant result to retain here is the very small range of the I_p values obtained (experimentally and theoretically) for the three compounds, which is principally due to the similar nature of their HOMO orbitals.

Charge-transporting properties

The hole-transporting properties of the amorphous layers of **FFF**, **CFC** and **FCF** were studied by a time-of-flight (TOF) technique in the xerographic regime. The xerographic TOF transients for a thin layer of **FFF** and **CFC1** are shown in Fig. 7. The transients of the layers of **FFF** are with a well-defined transit time on the linear plots. Similar transients were observed for the compound end-capped with fluorene moieties (**FCF**). These observations show that non-dispersive hole transport is characteristic of the layers **FFF** and **FCF**. In contrast to fluorene end-capped compounds the dispersive charge transport was observed for the layers of a carbazole end-capped compound (**CFC1**). No transit times were observed in the linear plots, however they were well seen on lg–lg plots. Similar transients were observed for the layers of **CFC2**.

The dependencies of the hole drift mobilities (μ) on the square root of the electric field for all four compounds are shown in Fig. 8, and the hole drift mobility in the electric field of 6.4×10^5 V cm^{-1} are summarized in Table 4.

The change of the alkyl substituent from 2-ethylhexyl (**CFC1**) to hexyl (**CFC2**) resulted in higher TOF hole mobilities.

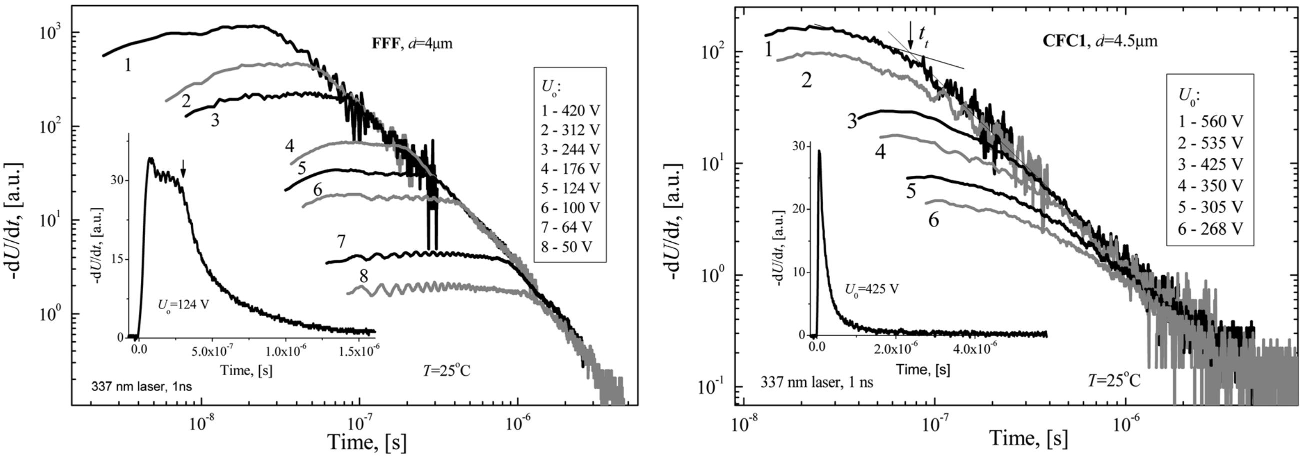

Fig. 7 Xerographic time of flight transients for amorphous films of **FFF** and **CFC1**. The insets show one transient curve in the linear plot.

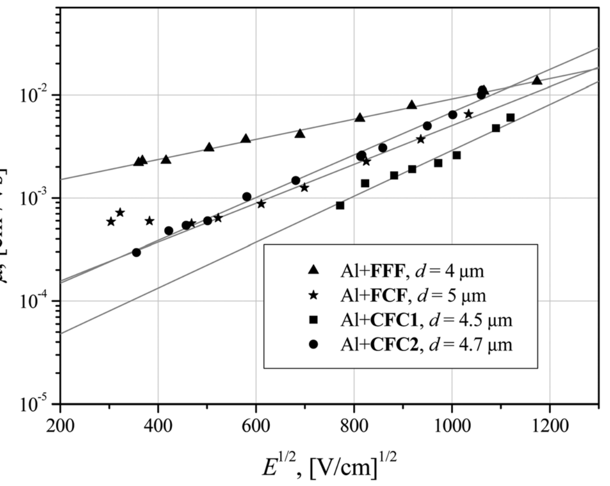

Fig. 8 Hole drift mobilities as a function of $E^{1/2}$ for layers of **CFC**, **FCF**, **FFF**.

The hole-transport properties of these compounds can be compared in the frame of the Marcus theory.[17–20] In the case of amorphous materials, the rate-constant of a hole-transfer reaction between two adjacent molecules can be described by the "hopping" mechanism and the calculated mean of the following equation:

$$k_{\mathrm{HT}} = \frac{4\pi^2}{h}\frac{1}{\sqrt{4\pi\lambda k_{\mathrm{B}}T}}t^2 \exp\left[\frac{-(\Delta G^{\mathrm{o}} + \lambda)^2}{4k_{\mathrm{B}}\lambda T}\right] \qquad (1)$$

where t is the electronic coupling between two adjacent molecules, ΔG^{o} is the free energy of the hole-transfer reaction, and λ is the reorganization energy. This last parameter contains contributions from the medium polarization energy (λ_{s}), and from the energetic effort due to the intra-molecular geometric relaxations related to the hole transfer between two adjacent molecules (λ_{i}).

Eqn (1) indicates that in order to obtain high hole-transfer rate-constants (k_{HT}), the reorganization energy (λ) should be small whereas the electronic coupling parameter (t) should be large. In the following only these two molecular parameters will be discussed.

The results shown in Table 4 indicate larger reorganization energies for electron transport than for holes, suggesting that, based on this factor only, the electron transport should be only slightly inferior as compared to the holes. The internal reorganization energy (λ_{i}) values of **H-CFC**, **H-FCF**, and **H-FFF** corresponding to the hole transport are relatively small (0.221, 0.216, and 0.215 eV, respectively, Table 4), which is in line with the high hole mobilities recorded for these compounds, and very similar between them, consistent with the quite similar hole mobilities. (This statement remains unchanged if the reorganization energies of "half-compounds" are considered instead of those presented in Table 4. See ref. 46 for additional details.) Table S1 (ESI†) indicates that this trend is unchanged and the absolute values are only slightly modified if alkyl groups are considered instead of hydrogen atoms. On the other hand, the quite similar shapes and localization of HOMO orbitals for the three compounds (Fig. 2 and Fig. S1, ESI†) suggest that, based only on this factor (thus ignoring the steric effect of alkyl groups), similar transfer integrals would be expected, which is in line with the suggestions deduced from the comparison of the reorganization energies. We also remember that the HOMO orbitals (Fig. 2 and Fig. S1, ESI†) are distributed over the whole molecular backbones with still non-negligible contributions from the peripheral rings, thus suggesting a potential for non-negligible transfer integrals between adjacent molecules in the films. Good and similar intrinsic hole transport properties could consequently be predicted for these materials, suggesting that differences in their performances should be dominated by other properties.

Table 4 Xerographic time of flight hole mobilities for layers of **CFC1**, **CFC2**, **FCF**, and **FFF**. The intramolecular reorganization energies for hole- and electron-transport (corresponding to the model compounds **H-CFC**, **H-FCF**, and **H-FFF**) as calculated at the B3LYP/6-31G(d,p) level are also shown

Compound	**CFC1**	**CFC2**	**FCF**	**FFF**
μ [cm^2 V^{-1} s^{-1}]	1.0×10^{-3}	2.6×10^{-3}	2.2×10^{-3}	5.7×10^{-3}
$\lambda_{\mathrm{i}}^{\mathrm{h}}$ [eV]		0.221	0.216	0.215
$\lambda_{\mathrm{i}}^{\mathrm{e}}$ [eV]		0.288	0.276	0.291

Despite the abovementioned similarities, the charge transport properties of these compounds are found to be strongly influenced by other factors, such as possible differences in the intermolecular interactions or presence of charge traps and other disorder sources. Indeed, disorder-dominated hole transport has been deduced in the case of polyfluorene copolymers,[47] which could give an indication of the hole transport properties in the case of **FFF**. The dispersive TOF signal observed for **CFC** (Fig. 7) indicates that the measured value corresponds to a maximum hole-mobility instead of an average value,[48] suggesting that charge transport in **CFC** is less efficient as compared to **FCF** and **FFF**. The higher dipole moment of **H-CFC** (by 3–4 times) as compared to those of **H-FCF** and **H-FFF** is for instance expected to enlarge the density of states and degrade the hole transport in this case.[49–51] It is worth noting that this last factor is found to be only slightly dependent on the nature of the real alkyl chains across the series (Table S2, ESI†). As for the differences between the charge transport properties of **FCF** and **FFF**, this might be explained in part by the differences in the molecular packing due to the alkyl chain groups. The importance of this effect is quite visible from the important increase in the hole mobility of **CFC2** as compared to **CFC1**. A possible explanation for this last difference could be related to the more hindering alkyl groups in **CFC1** (Scheme 1 and Fig. 1d and e) which prevents a good spatial approach between two adjacent molecules, thus reducing the transfer integrals and hole hopping between them. However, the difference in the hole-mobilities between **CFC1** and **CFC2** might also be influenced by the presence of accidental charge traps in **CFC1**.

Conclusions

We have synthesized a series of trimers consisting of carbazole and fluorene moieties which exhibit high thermal stabilities and form molecular glasses. Cyclic voltammetry revealed different electrochemical properties of the synthesized compounds. The fluorene trimer was found to be electrochemically stable. The oxidation of the trimers containing 2- and 2,7-substituted carbazole moieties was found to be irreversible, which is suspected to originate from the enhanced charge-localization propensity of these carbazole-derivatives in the oxidized state. The electron photoemission spectra of the amorphous films of the compounds revealed similar ionization potentials for **CFC** and **FFF** (5.83 and 5.89 eV, respectively) but a smaller value for **FCF** (5.65 eV). While the above similarity is explained by the similar intrinsic properties of **CFC** and **FFF**, the lower ionization potential of **FCF** is supposed to be related to stronger intermolecular interactions due to the smaller alkyl groups in the central core.

Hole drift mobilities in the layers of the synthesized compounds reached 10^{-2} cm^2 V^{-1} s^{-1} at high electric fields. The hole mobility in **CFC** compound is found to be less efficient as compared to **FCF** and **FFF**, regardless of the similar values obtained from TOF measurements.

Except for some differences in the dipole moment, the theoretical results corresponding to neutral isolated molecules suggest quite similar geometries for the three compounds, similar HOMO and LUMO shape and energy, and very similar absorption and fluorescence spectra. These intrinsic properties are found to be insignificantly dependent on the nature of alkyl groups. Consequently, the smaller optical absorption intensities found experimentally for **CFC** and **FCF** as compared to **FFF**, along with the lower ionization potential of **FCF** and the less efficient hole transport properties of **CFC1** and **CFC2** are supposed to stem from other effects dominating the intrinsic molecular properties, such as differences in dipole moments and/or different packing manners in the condensed state of these molecules.

Acknowledgements

This research was supported by FP7 REGPOT-2012-2013-1 ICT Project CEOSeR (Grant Agreement 316010). We thank Habil. Dr V. Gaidelis for help with ionization potential measurements.

References

1 M. T. Bernius, M. Inbasekaran, J. O'Brien and W. Wu, *Adv. Mater.*, 2000, **12**, 1737–1750.
2 W. Wu, Y. Liu and D. Zhu, *Chem. Soc. Rev.*, 2010, **39**, 1489–1502.
3 B. C. Thompson, Y. G. Kim, T. D. McCarley and J. R. Reynolds, *J. Am. Chem. Soc.*, 2006, **128**, 12714–12725.
4 A. Tomkeviciene, J. V. Grazulevicius, K. Kazlauskas, A. Gruodis, S. Jursenas, T. H. Ke and C. C. Wu, *J. Phys. Chem. C*, 2011, **115**, 4887–4897.
5 Y. M. Tao, H. Y. Li, Q. L. Xu, Y. C. Zhu, L. C. Kang, Y. X. Zheng, J. L. Zuo and X. Z. You, *Synth. Met.*, 2011, **161**, 718–723.
6 B. K. Yap, R. D. Xia, M. Campoy-Quiles, P. N. Stavrinou and D. D. C. Bradley, *Nat. Mater.*, 2008, **7**, 376–380.
7 K. T. Wong, Y. Y. Chien, T. T. Chen, C. F. Wang, Y. T. Lin, H. H. Chiang, P. Y. Hsieh, C. C. Wu, C. H. Chou and Y. O. Su, *et al.*, *J. Am. Chem. Soc.*, 2002, **124**, 11576–11577.
8 C. C. Wu, T. L. Liu, W. Y. Hung, Y. T. Lin, K. T. Wong, R. T. Chen, Y. M. Chen and Y. Y. Chien, *J. Am. Chem. Soc.*, 2003, **125**, 3710–3711.
9 J. F. Morin, M. Leclerc, D. Ades and A. Siove, *Macromol. Rapid Commun.*, 2005, **26**, 761–778.
10 M. Leclerc, *J. Polym. Sci., Part A: Polym. Chem.*, 2001, **39**, 2867–2873.
11 J.-Y. Shen, X.-L. Yang, T.-H. Huang, J. T. Lin, T.-H. Ke, L. Y. Chen, C.-C. Wu and M.-C. P. Yeh, *Adv. Funct. Mater.*, 2007, **17**, 983–995.
12 M. Sonntag and P. Strohriegl, *Chem. Mater.*, 2004, **16**, 4736–4742.
13 R. Karpicz, S. Puzinas, J. Sulskus, S. Grigalevicius and V. Gulbinas, *Chem. Phys.*, 2012, **404**, 82–87.
14 G. Zotti, G. Schiavon, S. Zecchin, J.-F. Morin and M. Leclerc, *Macromolecules*, 2002, **35**, 2122–2128.
15 J.-F. Morin and M. Leclerc, *Macromolecules*, 2002, **35**, 8413–8417.
16 F. Dierschke, A. C. Grimsdale and K. Müllen, *Synthesis*, 2003, 2470–2472.
17 R. A. Marcus, *J. Chem. Phys.*, 1956, **24**, 966–978.
18 R. A. Marcus, *Rev. Mod. Phys.*, 1993, **65**, 599–610.
19 R. A. Marcus and N. Sutin, *Biochim. Biophys. Acta*, 1985, **811**, 265–322.
20 V. G. Levich, *Adv. Electrochem. Electrochem. Eng.*, 1966, **4**, 249–371.
21 T. Malinauskas, M. Daskeviciene, K. Kazlauskas, H. C. Su, J. V. Grazulevicius, S. Jursenas, C. C. Wu and V. Getautis, *Tetrahedron*, 2011, **67**, 1852–1861.
22 E. Miyamoto, Y. Yamaguchi and M. Yokoyama, *Electrophotography*, 1989, **28**, 364–370.
23 E. Montrimas, V. Gaidelis and A. Pazera, *Lith. J. Phys.*, 1996, **6**, 569–578.
24 S. M. Vaezi-Nejad, *Int. J. Electron.*, 1987, **62**, 361–384.
25 A. Matoliukstyte, J. V. Grazulevicius and V. Jankauskas, *Mol. Cryst. Liq. Cryst.*, 2007, **466**, 85–100.
26 M. Lux, P. Strohriegl and H. Hoecker, *Macromol. Chem.*, 1987, **188**, 811–820.
27 W. W. Limburg, J. F. Yanus, D. J. Williams, A. O. Goedde and J. M. Pearson, *J. Polym. Sci., Polym. Chem. Ed.*, 1975, **13**, 1129–1133.
28 H. Thiem, P. Strohriegl, S. Setayesh and D. Leeuw, *Synth. Met.*, 2006, **156**, 582–589.
29 P. L. Burn, A. Kraft, D. R. Baigent, D. D. C. Bradley, A. R. Brown, R. H. Friend, R. W. Gymer, A. B. Holmes and R. W. Jackson, *J. Am. Chem. Soc.*, 1993, **115**, 10117–10124.
30 A. Kruzinauskiene, A. Matoliukstyte, A. Michaleviciute, J. V. Grazulevicius, J. Musnickas, V. Gaidelis and V. Janakuskas, *Synth. Met.*, 2007, **157**, 401–406.
31 W. Kohn and L. J. Sham, *Phys. Rev.*, 1965, **140**, A1133–A1138.
32 C. Lee, W. Yang and R. G. Parr, *Phys. Rev. B: Condens. Matter Mater. Phys.*, 1988, **37**, 785–789.

33 A. D. Becke, *J. Chem. Phys.*, 1993, **98**, 5648–5652.
34 E. K. U. Gross and W. Kohn, *Phys. Rev. Lett.*, 1985, **55**, 2850–2852.
35 E. K. U. Gross and W. Kohn, *Adv. Quantum Chem.*, 1990, **21**, 255–291.
36 R. Bauernschmitt and R. Ahlrichs, *Chem. Phys. Lett.*, 1996, **256**, 454–464.
37 M. E. Casida, C. Jamorski, K. C. Casida and D. R. Salahub, *J. Chem. Phys.*, 1998, **108**, 4439–4449.
38 R. Dennington, T. Keith and J. Millam, *GaussView, Version, 5*, Semichem Inc., Shawnee Mission KS, 2009.
39 J. L. Bredas, D. Beljonne, V. Coropceanu and J. Cornil, *Chem. Rev.*, 2004, **104**, 4971–5003.
40 V. Barone and M. Cossi, *J. Phys. Chem. A*, 1998, **102**, 1995–2001.
41 M. Cossi, N. Rega, G. Scalmani and V. Barone, *J. Comput. Chem.*, 2003, **24**, 669–681.
42 M. J. Frisch, G. W. Trucks, H. B. Schlegel, G. E. Scuseria, M. A. Robb, J. R. Cheeseman, G. Scalmani, V. Barone, B. Mennucci and G. A. Petersson, *et al.*, *Gaussian 09, Revision B.01*, Gaussian Inc., Wallingford CT, 2010.
43 J. Qu, Y. Suzuki, M. Shiotsuki, F. Sanda and T. Masuda, *Polymer*, 2007, **48**, 4628–4636.
44 A. Tomkeviciene, G. Puckyte, J. V. Grazulevicius, M. Degbia, F. Tran-Van, B. Schmaltz, V. Jankauskas and J. Boucle, *Synth. Met.*, 2012, **162**, 1997–2004.
45 G. Zotti, G. Schiavon, S. Zecchin, J. F. Morin and M. Leclerc, *Macromolecules*, 2002, **35**, 2122–2128.
46 Another indication on the charge-localization *versus* charge-delocalization comes from the electronic coupling between the local HOMO of each individual carbazole unity in **H-CFC**. Our results indicate an electronic coupling of 0.23 eV, which is slightly smaller than the intramolecular reorganization energy (0.27 eV) of a ‘‘half’’-compound (carbazole-fluorene instead of **CFC**). In the case of **H-FFF**, a coupling of 0.24 eV is found as compared to 0.25 eV for the reorganization energy of the ‘‘half’’ compound. Potential for charge localization in the oxidized state is suggested, slightly less pronounced in the case of **H-FFF**. The electronic coupling is estimated as half the energy difference between two occupied orbitals of **H-CFC** (**H-FFF**), corresponding to the in-phase and to the out-of-phase combinations of the local HOMOs.
47 S. L. M. van Mensfoort, S. I. E. Vulto, R. A. J. Janssen and R. Coehoorn, *Phys. Rev. B: Condens. Matter Mater. Phys.*, 2008, **78**, 085208.
48 H. Baessler and A. Koehler, *Top. Curr. Chem.*, 2012, **312**, 1–66.
49 P. M. Borsenberger and H. Bassler, *J. Chem. Phys.*, 1991, **95**, 5327–5331.
50 J. L. Maldonado, M. Bishop, C. Fuentes-Hernandez, P. Caron, B. Domercq, Y. D. Zhang, S. Barlow, S. Thayumanavan, M. Malagoli and J. L. Bredas, *et al.*, *Chem. Mater.*, 2003, **15**, 994–999.
51 D. K. Oh, S. M. Hong, C. E. Lee, B. S. Kim and J. I. Jin, *Solid State Commun.*, 2005, **136**, 585–590.